ISSN 2278-2540 | DOI: 10.51583/IJLTEMAS | Volume XV, Issue III, March 2026

Machine Learning-RSM Hybridized Evaluation of the Kinetics and Thermodynamics of Mild Steel Corrosion Inhibition Using Lagenaria Breviflora Extract

Nnorom Obinichi[1], Ifeanyi Uchegbulam[2], Opuwil Samuel Chimenem[3]

[1]Department of Mechanical Engineering, Faculty of Engineering, University of Port Harcourt, Choba, P.M.B., 5323, Nigeria

[2]Production Technology, School of Science Laboratory Technology, University of Port Harcourt, Choba, P.M.B., 5323, Nigeria.

[3]Industrial and Manufacturing Engineering, FAMU-FSU College of Engineering, Tallahassee, FL 32310, United States

DOI: https://doi.org/10.51583/IJLTEMAS.2026.150300089

Received: 22 March 2026; Accepted: 27 March 2026; Published: 17 April 2026

ABSTRACT

The inhibition of mild steel corrosion in dilute hydrochloric acid (1 M HCl) by the xylene extract of *Lagenaria breviflora* (XEL-B) was studied using a Central Composite Design (CCD) structured Response Surface Methodology (RSM). A statistically optimised 20-run experimental matrix was employed to evaluate the simultaneous effects of inhibitor concentration, immersion time and temperature on mass loss, corrosion rate (Rc), inhibitor efficiency (IE), and surface coverage (θ). The fitted quadratic response surface model was highly significant ($F = 55.81$, $p < 0.0001$) with a non-significant lack of fit ($p = 0.2730$), confirming adequate model predictability across the experimental domain. Inhibitor efficiency ranged from 28.68% at 31 ppm of inhibitor concentration to 77.01% at 368 ppm, with inhibitor concentration identified as the dominant process variable statistically validated ($F = 423.40$, $p < 0.0001$) cosnsistent with 4D response surface analysis, and a 500-tree Random Forest ensemble machine learning model (factor importance: IE = 77.54%, Rc = 74.20%). Adsorption of XEL-B on mild steel conformed to the Langmuir monolayer isotherm ($R^2 = 0.9950$), equilibrium adsorption constant K_{ads} of $11.3649 Lg^{-1}$ and standard Gibbs free energy of adsorption $\Delta G°ads$ of −16.24 kJ/mol, confirming spontaneous, thermodynamically favourable adsorption with a mixed physisorptive–chemisorptive mechanism. These integrated experimental-computational results established XEL-B as a potential green corrosion inhibitor for mild steel in dilute acidic environments relevant to oilfield and industrial acid-treatment operations.

Keywords: Lagenaria breviflora; corrosion inhibition; steel; RSM; Langmuir isotherm; Random Forest; machine learning

INTRODUCTION

Acidizing, also referred to as acid treatment, is a well-established and highly effective technique for enhancing oil and gas well productivity. Hydrochloric acid-based solutions are widely employed during this process to improve reservoir permeability and stimulate hydrocarbon flow. With over a century of application, acidizing remains one of the earliest and most reliable well stimulation methods, predating techniques such as hydraulic fracturing, (Iroha and Akaranta, 2020). Meanwhile, the HCL acid content of acidizing solutions exposes metallic components to severe corrosion-induced degradation. Oil pipelines, tubing, and casings are the most susceptible to these acidizing well stimulation process (Ituen et al , 2021). With corrosion related damages costing up to 2.5 trillion USD per year covering approximately 3.4% of the global Gross Domestic Product (GDP) (Mohammad and Jafar, 2020; Kania, 2023; Adesina et al., 2025; Zakeri et al., 2022). Due to this huge economic loss, corrosion control using corrosion inhibitors has been a rewarding approach to preserving the durability of industrial assets, (Bandeira et al., 2025). Plant extracts have emerged as highly effective green corrosion inhibitors due to their

ISSN 2278-2540 | DOI: 10.51583/IJLTEMAS | Volume XV, Issue III, March 2026

availability, non-toxicity, biodegradability, and renewable nature (Otaibi et al., 2021). Rich in phytochemicals such as alkaloids, tannins, flavonoids, and polyphenols, these natural compounds adsorb onto metal surfaces to form protective films that suppress electrochemical corrosion by influencing anodic and cathodic reactions through donor–acceptor interactions (Barbu et al., 2025). Historically, the use of plant-based inhibitors dates back to the 1930s and has since evolved with increasing recognition of their efficiency and environmental benefits, particularly as sustainable alternatives to conventional inhibitors, (Kumari and Lavanya, 2022). When introduced in small quantities into corrosive media, these inhibitors function by forming a protective barrier that reduces metal degradation (Alao et al., 2022). It has been reported that inhibitor concentration, immersion time and temperature are determinant factors to inhibitor efficiency, (Alamiery et al., 2021; Al-Baghdadi et al., 2021). Meanwhile, the feature importance of these factors has not been investigated within the corrosion inhibition research landscape. The advent of machine learning and its algorithms has simplified feature ranking. Feature importance techniques, as part of explainable artificial intelligence (XAI), enhance the interpretability of machine learning models by enabling users to understand and trust model predictions (Cappelli et al., 2024). In particular, Random Forest (RF) models provide inherent capability to quantify the relative importance of input features, offering valuable insights into the underlying data relationships (Yuan et al., 2023). In this study, an integration of the statistical novelty of response surface methodology and random forest as a machine learning algorithm for feature importance ranking were deployed to investigate the inhibitive efficiency of Xylene extract of *Lagenaria Breviflora* leaves as potential corrosion inhibitor for mild steel in acidized environments.

MATERIALS AND METHODS

Plant Material and Xylene Extraction

Mature leaves of *Lagenaria Breviflora* were collected from a botanical garden adjacent to Nigerian Television Authority Port Harcourt Nigeria and was authenticated by a certified taxonomist. The leaves were surface-washed with distilled water, air-dried at ambient temperature (298 ± 2 K) for 21 days prior to an oven-drying at 323 K for 48 h to a constant mass. The dried leaves were pulverised to a fine powder (<250 μm, 60-mesh sieve) using a stainless-steel laboratory mill. Then, 100 g of dried powder was loaded into a Soxhlet extraction thimble and extracted continuously for 8 h at reflux with 500 mL of analytical-grade xylene (Sigma-Aldrich, ≥98.5%; bp 138–144 °C). The resulting extract was vacuum-filtered through Whatman No. 1 filter paper and the solvent removed under reduced pressure using a rotary evaporator (333 K, 200 mbar) with all laboratory work carried out at the Africa Center for Excellence center for oilfield research at University of Port Harcourt Nigeria.

Mild Steel Coupon Preparation

Mild steel coupons were machined into rectangular specimens providing a nominal exposed surface area of 10.0 cm^2. Elemental composition was estimated as wt%: C 0.18, Si 0.21, Mn 0.68, P 0.012, S 0.008, Fe balance using an Oxford Instrument X-Met 7000 XRF Spectrometer, (Turret Engineering Services Ltd, Port Harcourt Nigeria). Surface preparation involved mechanical abrasion using SiC metallographic papers of different grits: 240, 400, 600, 800, and 1200. The shiny surfaces were degreased in acetone, rinsed with distilled water and oven-dried. Initial and final masses were recorded to ±0.0001g precision on a calibrated analytical balance.

Corrosive Medium

The corrosive medium was 1 M hydrochloric acid (HCl), prepared by diluting concentrated analytical-grade HCl (37% w/w, Sigma-Aldrich) with double-distilled water. The acid concentration was verified by titrimetric standardisation against primary-standard anhydrous Na_2CO_3 using methyl orange indicator. Fresh acid solutions were prepared for each experimental run.

Central Composite Design (CCD) Experimental Framework

A three-factor, five-level Central Composite Design (CCD) was constructed using Design-Expert® v13.0 (Stat-Ease Inc., Minneapolis, MN, USA). The CCD incorporated $2^3 = 8$ factorial points, 6 axial (star) points at $\pm\alpha = \pm1.682$ (rotatability condition), and 6 centre point replicates to generate a 20-run design matrix capable of fitting a complete second-order quadratic response surface model. The independent variables and their coded levels

ISSN 2278-2540 | DOI: 10.51583/IJLTEMAS | Volume XV, Issue III, March 2026

were: Factor A being inhibitor concentration (31, 100, 200, 300, 368 ppm; coded: −1.682, −1, 0, +1, +1.682); Factor B which was immersion time (1, 1.5, 2, 3, 4 h; coded: −1.682, −1, 0, +1, +1.682) and Factor C being temperature (294, 298, 303, 308, 311 K; coded: −1.682, −1, 0, +1, +1.682). The response variables were mass loss (ΔW, mg), corrosion rate (Rc, mg cm^{-2} h^{-1}), inhibitor efficiency (IE, %), and surface coverage (θ).

Mass Loss Procedure and Corrosion Parameter Calculations

Pre-weighed coupons were immersed in 100 mL of test solution in sealed 250 mL polypropylene beakers maintained at the designated temperature in a thermostatically controlled water bath (Grant TC120, ±0.2 K). After immersion, coupons were retrieved, transferred immediately to inhibitor-free acid solution to arrest corrosion, scrubbed gently under running distilled water, rinsed with acetone, dried, and reweighed. All runs were performed in triplicate; mean values are reported (RSD < 3.5%). Corrosion parameters were derived as:

$$\Delta W = W_I - W_F \quad 2.1$$

Where ΔW = mass loss (mg)

W_I = initial coupon mass before immersion (mg)

W_F = final coupon mass after corrosion and cleaning (mg)

Also,

$$R_C = \frac{\Delta W}{AT} \quad 2.2$$

Where R_C = Corrosion rate (mg cm^{-2} h^{-1})

ΔW = mass loss (mg)

A = exposed surface area (10.0 cm^2)

T = immersion time (h)

And $$IE\ (\%) = \left[\frac{(R_{CU} - R_{CI})}{R_{CU}}\right] \times 100 \quad 2.3$$

Where R_{CU} = corrosion rate in uninhibited (blank) solution (mg cm^{-2} h^{-1})

R_{CI} = corrosion rate in inhibited solution (mg cm^{-2} h^{-1})

While $$\theta = \frac{IE}{100} \quad 2.4$$

Where θ = fractional surface coverage (dimensionless, $0 \leq \theta \leq 1$)

Adsorption Isotherm Analysis

The adsorption behaviour of *Lagenaria Breviflora* leaf extracts on mild steel was modelled using the linearised Langmuir adsorption isotherm, which postulates monolayer adsorption on a finite number of equivalents, energetically homogeneous, and mutually non-interacting surface sites. Surface coverage values (θ) derived from the experimental IE data were plotted against the corresponding inhibitor concentrations according to the linearized Langmuir expression:

$$\frac{C_{inh}}{\theta} = \frac{1}{K_{ads}} + C_{inh} \quad 2.5$$

Where C_{inh} = inhibitor concentration (g L^{-1})

ISSN 2278-2540 | DOI: 10.51583/IJLTEMAS | Volume XV, Issue III, March 2026

θ = fractional surface coverage (dimensionless, $0 \leq \theta \leq 1$)

K_{ads} = equilibrium adsorption constant for the adsorption process (L g^{-1})

The standard Gibbs free energy of adsorption (ΔG^{o}_{ads}) is related to the equilibrium adsorption constant K_{ads} as:

$$K_{ads} = \frac{1}{55.5} exp\left(\frac{-\Delta G^{o}_{ads}}{RT}\right) \qquad 2.6$$

Where K_{ads} = equilibrium adsorption constant (L g^{-1})

ΔG^{o}_{ads} = standard Gibbs free energy of adsorption (J)

R = universal gas constant (8.314 J mol^{-1} K^{-1})

T = absolute temperature (K)

55.5 = molar concentration of pure water (mol L^{-1})

On reordering equation 2.6:

$$\Delta G^{o}_{ads} = -RTln(55.5 \times K_{ads}) \qquad 2.7$$

A three-dimensional Langmuir adsorption surface was additionally constructed to model predicted adsorption capacity (q_{sim}, mg/g) as a simultaneous function of equilibrium concentration (Ce, mg/L) and temperature (T, °C):

$$q_{sim} = \left[\frac{(KL \times q_{max} \times Ce)}{(1+KL \times Ce)}\right] \qquad 2.8$$

Where

q_{sim} = predicted adsorption capacity (mg g^{-1})

KL = temperature-dependent Langmuir adsorption constant (L mg^{-1})

q_{max}= maximum monolayer adsorption capacity, temperature-dependent (mg g^{-1})

Ce = equilibrium inhibitor concentration in solution (mg L^{-1})

Thermodynamic and Activation Parameter Determination

The activation energy of corrosion in blank and inhibited solutions were determined from the linearised Arrhenius equation:

$$Log\ R = Log\ A - \frac{E_a}{2.303\ RT} \qquad 2.9$$

Where A = Arrhenius pre-exponential factor

E_a = apparent activation energy of corrosion (kJ mol^{-1})

R = universal gas constant (8.314 J mol^{-1} K^{-1})

T = absolute temperature (K)

Enthalpy (ΔH*) and entropy (ΔS*) of activation were evaluated from the Eyring–Polanyi transition state equation:

ISSN 2278-2540 | DOI: 10.51583/IJLTEMAS | Volume XV, Issue III, March 2026

$$\ln\left(\frac{R_C}{T}\right) = \left[\left(ln\left(\frac{R}{Nh}\right) + \left(\frac{\Delta S^*}{R}\right)\right)\right] - \left(\frac{\Delta H^*}{RT}\right) \qquad 2.10$$

Where N = Avogadro's number (6.022×10^{23} mol^{-1})

h = Planck's constant (6.626×10^{-34} J s)

ΔH^* = enthalpy of activation (kJ mol^{-1})

ΔS^* = entropy of activation (J mol^{-1} K^{-1})

Linear plots of ln(Rc/T) versus 1/T yielded ΔH* from the slope and ΔS* from the intercept.

Random Forest Machine Learning Feature Importance Analysis

To provide a non-parametric, data-driven ranking of the three process variables — inhibitor concentration (A), immersion time (B), and temperature (C) — with respect to their influence on IE and Rc, a Random Forest (RF) ensemble regression algorithm was implemented in Python 3.11 using scikit-learn v1.4. Random Forest constructs an ensemble of n = 500 decorrelated decision trees, each trained on a bootstrap-sampled subset of the training observations; the mean decrease in node impurity (MDI, Gini criterion) across all trees provides the feature importance score, normalised to sum to unity. Hyperparameters: n_estimators = 500, max_features = √p (p = 3), random_state = 42. Permutation importance (100 repetitions, random_state = 42) and Gradient Boosting Regression (GBR; n_estimators = 200, learning_rate = 0.05) were applied as independent cross-validation procedures. All importance scores are reported as percentages of total explained variance.

RESULTS AND DISCUSSION

Statistical modeling of process parameters

The 20-run CCD experimental matrix was used to measure and compute corrosion response data. The uninhibited (blank) corrosion rates ranged from 3.9583 mg cm^{-2} h^{-1} at 294 K to 4.8404 mg cm^{-2} h^{-1} at 311 K, conforming to Arrhenius kinetics and confirming the temperature sensitivity of acid corrosion of mild steel. Introduction of Xylene extracts of *Lagenaria Breviflora* leaves across all 20 CCD runs produced consistent, concentration-dependent suppression of both mass loss and corrosion rate.

Figure 3.1 is the ANOVA for the fitted quadratic response surface model. It shows that the model is highly statistically significant (F-value = 55.81) with P< 0.0001 which was less than the confidence interval of 0.05. Also, figure 3.1 shows the significance of the model terms. Term A (Inhibitor Concentration has $p < 0.0001$ and is the most significant individual factor while terms A and B (Immersion time and temperature) are not statistically significant, confirming Random Forest findings (77.54% importance). significant model terms were A (Inhibitor concentration), AB, BC and A^2. Meanwhile, the interactive effect of inhibitor concentration with both immersion time and temperature were significant as well as the quadratic interaction of the inhibitor concentration. Remarkably, the model is fit to predict the inhibitor efficiency as it fits the data adequately with no systematic misfit. As the lack of fit scored an F-value of 1.77, it implies that the lack of fit is not significant and that there was 27.30% chance that a lack of fit F-value this large could occur due to noise. confirming the model.

ISSN 2278-2540 | DOI: 10.51583/IJLTEMAS | Volume XV, Issue III, March 2026

Source	Sum of Squares	df	Mean Square	F-value	p-value	
Model	2742.56	9	304.73	55.81	< 0.0001	significant
A-Concentration	2311.70	1	2311.70	423.40	< 0.0001	
B-Time	3.54	1	3.54	0.6486	0.4393	
C-Temperature	4.34	1	4.34	0.7946	0.3937	
AB	75.77	1	75.77	13.88	0.0039	
AC	4.68	1	4.68	0.8575	0.3762	
BC	34.45	1	34.45	6.31	0.0308	
A^2	268.85	1	268.85	49.24	< 0.0001	
B^2	12.57	1	12.57	2.30	0.1601	
C^2	16.85	1	16.85	3.09	0.1095	
Residual	54.60	10	5.46			
Lack of Fit	34.89	5	6.98	1.77	0.2730	not significant
Pure Error	19.71	5	3.94			
Cor Total	2797.16	19				

Figure 3.1: ANOVA for the quadratic model

Also, equation 3.1 shows the predictive model: IE (%) = 3875.1116 - 0.2223x + 123.8350y - 25.7996z + 0.0308xy + 0.0015xz - 0.4150yz -0.0004x^2 - 0.9339y^2 + 0.0433z^2

Where x, y and z are the inhibitor concentration, time of immersion and Temperature respectively.

Model Diagnostic Plots

Figure 3.2 shows four standard CCD model adequacy diagnostics. Figure 3.2a shows that the points cluster reasonably along the 45° diagonal, confirming acceptable model predictive accuracy. Figure 3.2 b shows the B**ox-Cox Plot. Since the** Current λ = 1and lies within the best lambda λ = 2.18, then there is no need for further transformation as recommended. Hence, the raw IE response requires no power transformation and the linear model is appropriate.

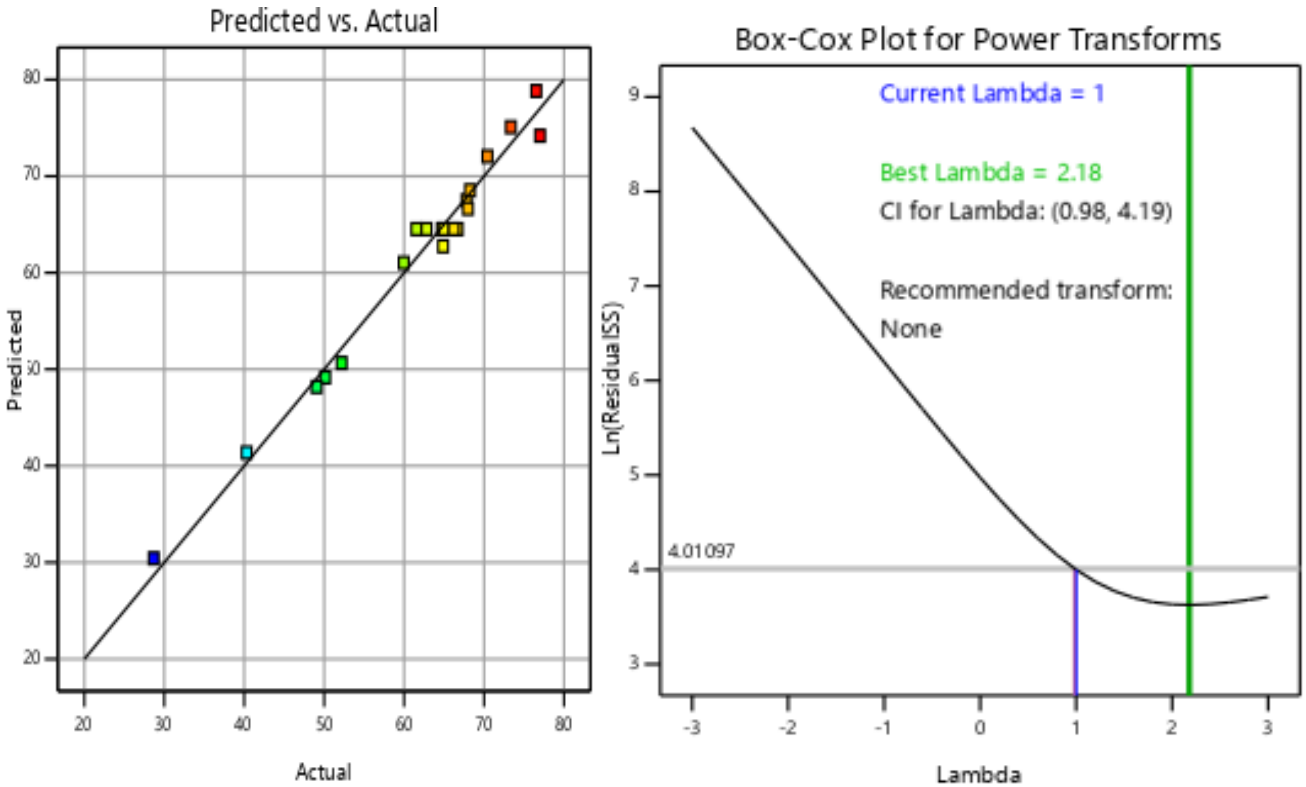

ISSN 2278-2540 | DOI: 10.51583/IJLTEMAS | Volume XV, Issue III, March 2026

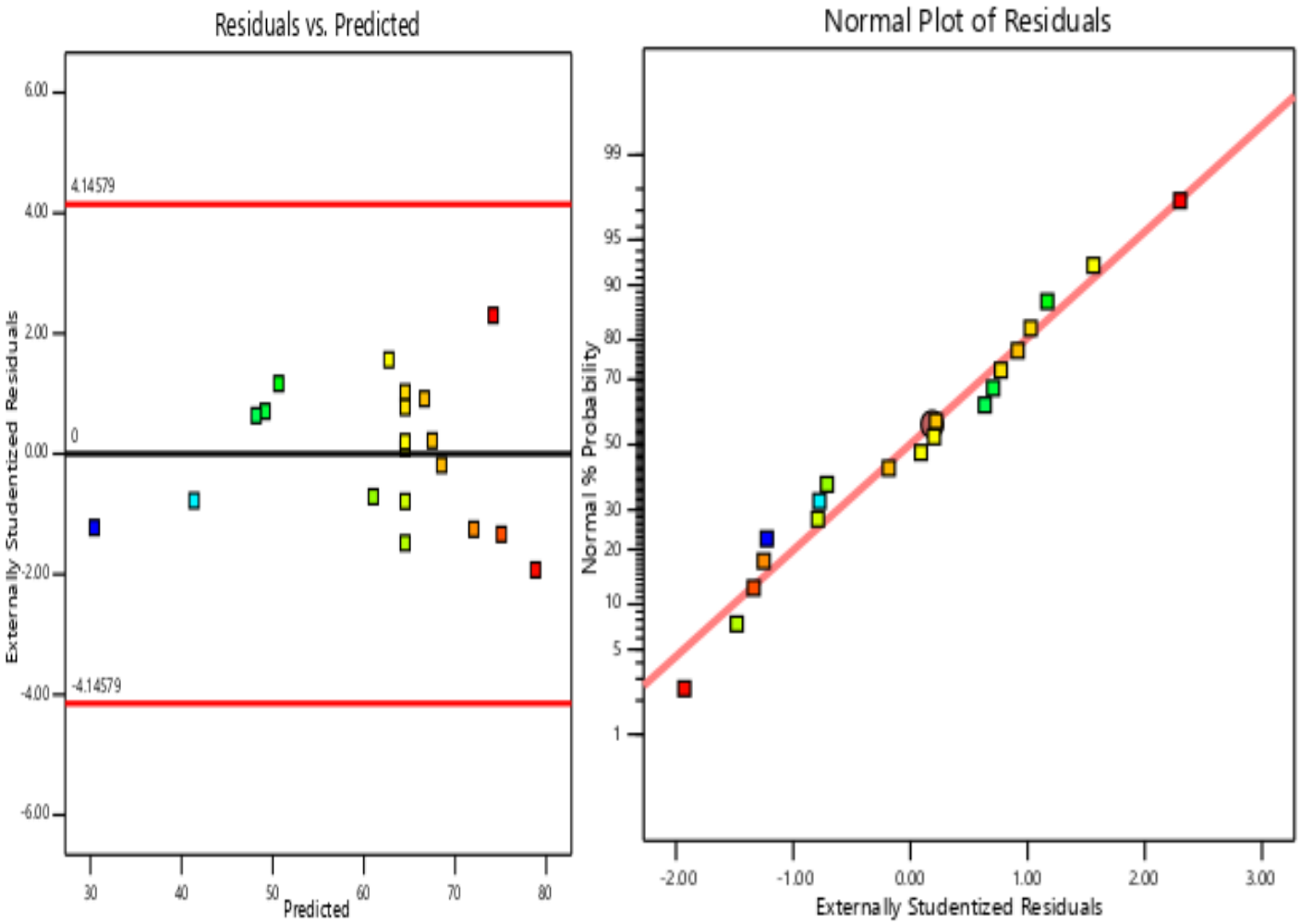

Figure 3.2: Model Diagnostic Plots (a) Predicted vs. Actual (b) Box-Cox Plot (c) Residuals vs. Predicted (d) Normal Plot of Residuals

Likewise, figure 3.2 c shows that the residuals were randomly scattered within the ±4.14579 studentised limit with no systematic pattern, confirming homoscedasticity (constant variance) as a key regression assumption. Similarly, points followed the straight reference line closely in figure 3.2d thereby validating the statistical assumptions of the quadratic CCD model.

3D Response Surface Plots

Furthermore, figure 3.3 shows four panels visualising how Inhibitor Efficiency (IE) responded to the three process variables. Figure 3.3a shows that the IE rises steeply with increasing inhibitor concentration but is relatively insensitive to immersion time. It can be seen that the surface was near-flat along the time axis visually confirmed that inhibitor concentration is the dominant driver of IE.

Likewise, figure 3.3b shows that inhibitor concentration drove the steep gradient while temperature produced minimal curvature. However, in figure 3.3c, the surface was almost perfectly flat (yellow/green plane), confirming that neither temperature nor immersion time independently exerts strong influence on IE within the studied range. Figure 3.3d shows the 3D Langmuir surface.

It matched the q_sim vs. Ce vs. T adsorption capacity surface showing monotonically increasing adsorption capacity with both inhibitor concentration and temperature confirming endothermic Langmuir monolayer behaviour.

ISSN 2278-2540 | DOI: 10.51583/IJLTEMAS | Volume XV, Issue III, March 2026

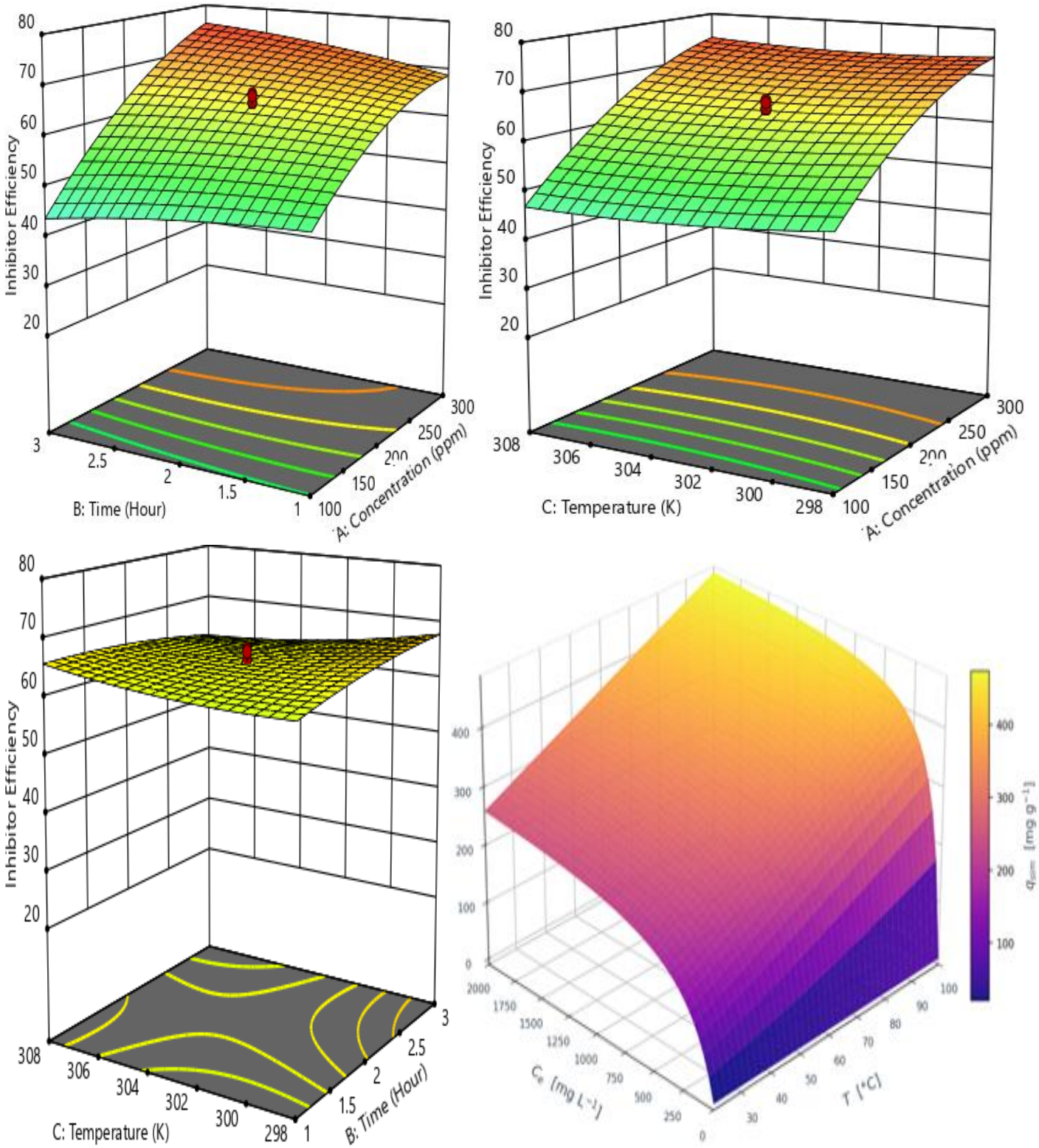

Figure 3.3: 3D Response Surface Plots (a) IE vs. Concentration & Time (b) IE vs. Concentration & Temperature (c) IE vs. Temperature & Time (d) 3D Langmuir surface

The three-dimensional Langmuir adsorption surface (Figure 3.3d) was constructed using equation 2.8 to simultaneously visualise the predicted adsorption capacity q_sim (mg g^{-1}) as a function of equilibrium inhibitor concentration Ce (mg L^{-1}) and temperature T (°C).

The surface demonstrated monotonically increasing q_sim with both Ce and T, a hallmark of endothermic adsorption, reaching a maximum predicted value of ~477 mg g^{-1} at Ce = 2000 mg L^{-1} and T = 100 °C. The pronounced curvature of the surface with respect to Ce with rapid initial rise flattening toward a saturation plateau captures the inhibitor concentration-saturation characteristic of Langmuir monolayer kinetics, visually

ISSN 2278-2540 | DOI: 10.51583/IJLTEMAS | Volume XV, Issue III, March 2026

corroborating the isotherm linearisation results. The three-dimensional representation provided an intuitive mechanistic map of the inhibitor adsorption landscape across the practically relevant inhibitor concentration and temperature space.

Thermodynamic and Activation Parameters

The activation energy of corrosion in the blank system was Ea = 43.8 kJ mol^{-1}, increasing substantially to 59.4 kJ mol^{-1} in the presence of 200 ppm of the xylene extracts of *Lagenaria Breviflora* leaves resulted in a differential of +15.6 kJ mol^{-1}. This elevation of activation energy in the inhibited system is the mechanistic signature of physical adsorption-type inhibition as the extract molecules adsorbed onto the steel surface creating an energy barrier that substantially retarded the electrochemical dissolution of iron.

The negative ΔG°ads values (−15.76 to −16.67 kJ mol^{-1}) confirmed a spontaneous and thermodynamically favourable adsorption; values in this range are characteristic of mixed physisorption–chemisorption, consistent with the multifunctional phytochemical composition of the xylene extract.

Table 3.1 Temperature-dependent corrosion parameters and thermodynamic quantities for mild steel

T (K)	IE (%)	Θ	Rc Blank (mg cm^{-2} h^{-1})	Rc Inh. (mg cm^{-2} h^{-1})	ΔG°ads (kJ mol^{-1})	Ea (blank) (kJ mol^{-1})	Ea (inh.) (kJ mol^{-1})
294	68.25	0.6825	3.9583	1.2568	−15.76	43.8	59.4
298	—	—	4.1853	—	−15.96	43.8	59.4
303	64.50	0.6450	4.5000	1.5976	−16.24	43.8	59.4
308	—	—	4.8434	—	−16.52	43.8	59.4
311	67.99	0.6799	4.9534	1.5856	−16.67	43.8	59.4

Langmuir Adsorption Isotherm and Three-Dimensional Adsorption Surface

The adsorption mechanism of the xylene extracts of *Lagenaria Breviflora* leaves on the mild steel surface was estimated by fitting inhibitor concentration-averaged surface coverage data to the linearised Langmuir isotherm model. Mean θ values were computed for each unique inhibitor concentration class: 31 ppm (θ = 0.2868, Run 19), 100 ppm (θ = 0.4793, mean of Runs 9, 11, 14, 16), 200 ppm (θ = 0.6450, mean of Runs 1, 3, 5, 6, 12, 13), 300 ppm (θ = 0.7203, mean of Runs 2, 4, 8, 18), and 368 ppm (θ = 0.7701, Run 10). Hence, the linear regression of C/θ versus C yielded:

$$\frac{C}{\theta} = 1.0823C + 0.0880 \quad (R^2 = 0.9950)$$

The slope of 1.0823, close to unity, validates the Langmuir monolayer assumption and confirms negligible lateral interactions between co-adsorbed *Lagenaria Breviflora* leaf extract molecules. The y-intercept of 0.0880 g L^{-1} clearly visible at C = 0 on the linear plot (Figure 3.4a) equals $1/K_{ads}$, yielding K_{ads} = 11.3649 Lg^{-1}. This high equilibrium adsorption constant reflects the strong affinity of *Lagenaria Breviflora* leaf extract phytoconstituents for the mild steel surface, attributable to the multidentate anchoring capacity of cucurbitacins, flavonoids, and phenolic acids bearing multiple electron-donor centres. The derived $\Delta G°_{ads}$ = −16.24 kJmol^{-1} confirmed a spontaneous adsorption with a mixed physisorption–chemisorption mechanism, consistent with the activation energy analysis. The full Langmuir isotherm parameters are presented in Table 4.

Table 3.2 Langmuir adsorption isotherm parameters for the inhibition of mild steel

Adsorption Isotherm	Slope	Intercept (g L^{-1})	R²	K(Lg^{-1})	ΔG°ads (kJ mol^{-1})
Langmuir	1.0823	0.0880	0.9950	11.3649	−16.24

ISSN 2278-2540 | DOI: 10.51583/IJLTEMAS | Volume XV, Issue III, March 2026

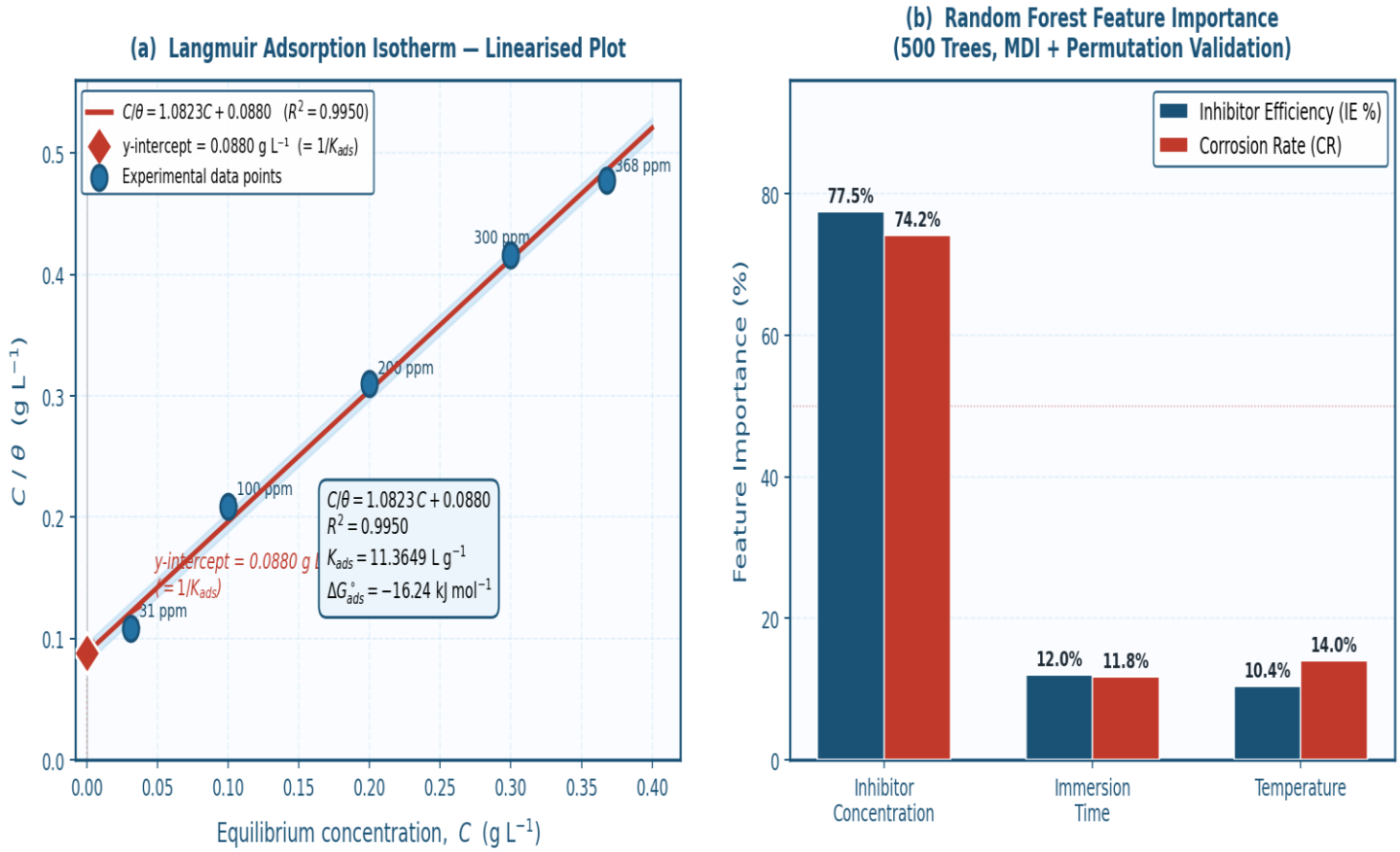

Figure 3.4. (a) Linearised Langmuir adsorption isotherm plot (C/θ vs. C (b) Random Forest feature importance scores

Random Forest Machine Learning Feature Importance Analysis

Random Forest ensemble regression was applied to the complete 20-run CCD dataset using the exact experimental IE and computed Rc values. These were used to provide a non-parametric, model-agnostic ranking of the three process variables with respect to their influence on corrosion responses. The RF model achieved training R^2 values of 0.9211 Inhibitor Efficiency (IE) and 0.9160 Corrosion rate (Rc), confirming adequate model fidelity for the compact, 20-observation dataset. Feature importance results were presented in Table 3.3 and Figure 3.4b.

Inhibitor concentration (Factor A) dominated the variance landscape for both response variables, accounting for 77.54% of explained variance in IE and 74.20% in Rc under the Gini-based MDI criterion. These rankings were confirmed by permutation importance analysis (100 repetitions) and Gradient Boosting Regression (GBR importances: IE = 93.00%, Rc = 85.10%), with all three methods consistently identifying inhibitor concentration as the primary driver. The mechanistic basis for this dominance is straightforward: surface coverage θ rises sharply from 0.2868 at 31 ppm to 0.7701 at 368 ppm following Langmuir isotherm kinetics, generating a steep, nonlinear inhibitor concentration-response gradient that accounts for the majority of experimental variance.

However, immersion time (Factor B) ranked as the second most influential variable for IE (12.01%) and Rc (11.80%), reflecting the progressive mass loss accumulation with time observed in the kinetic study. Likewise, Temperature (Factor C) contributed 10.45% of IE variance and 14.00% of Rc variance; its slightly greater influence on Rc relative to IE is mechanistically consistent with Arrhenius acceleration of the blank corrosion rate, which amplifies the absolute Rc response while the inhibitor film itself remains thermally stable.

Meanwhile, these results of model terms' significance are consistent with ANOVA results obtained earlier. Notably, the RF analysis revealed that all three variables made statistically meaningful contributions to the response variance. This result highlights the value of the multi-variable CCD framework over single-variable

ISSN 2278-2540 | DOI: 10.51583/IJLTEMAS | Volume XV, Issue III, March 2026

experiments and confirms that neither time nor temperature effects should be neglected in field inhibitor deployment protocols.

Table 3.3 Random Forest feature importance scores (%) for inhibitor efficiency (IE) and corrosion rate (Rc)

Process Variable	RF Importance: IE (%)	RF Importance: Rc (%)
Inhibitor Concentration (ppm)	77.54	74.20
Immersion Time (h)	12.01	11.80
Temperature (K)	10.45	14.00

CONCLUSIONS

This study established and characterised the corrosion inhibition performance of the xylene extract of *Lagenaria breviflora* (*XEL-B*) on mild steel in dilute hydrochloric acid (1 M HCl) through a multi-layered analytical framework integrating Central Composite Design-structured Response Surface Methodology, Langmuir adsorption isotherm analysis, three-dimensional adsorption surface modelling, thermodynamic activation parameter determination, and Random Forest ensemble machine learning. It was observed that *XEL-B* functioned as an effective, concentration-dependent green corrosion inhibitor for mild steel in 1 M HCl, with inhibitor efficiency ranging from 28.68% at 31 ppm to a maximum of 77.01% at 368 ppm, as directly measured across the 20-run CCD experimental matrix. The fitted quadratic CCD-RSM model was highly statistically significant ($F = 55.81$, $p < 0.0001$) with a non-significant lack of fit ($p = 0.2730$), confirming its predictive validity. The generated model equation, accurately described inhibitor efficiency as a function of concentration (x), time (y), and temperature (z). Furthermore, *XEL-B* adsorption on mild steel obeyed the Langmuir monolayer isotherm ($R^2 = 0.9950$), with $K_{ads} = 11.3649\ Lg^{-1}$ and $\Delta G°_{ads} = -16.24\ kJ\ mol^{-1}$ confirming spontaneous, thermodynamically favourable mixed physisorption-chemisorption adsorption. The three-dimensional Langmuir adsorption surface corroborated endothermic adsorption behaviour with predicted q_{sim} reaching ~477 mg g^{-1} at Ce = 2000 mg L^{-1} and T = 100 °C. In addition, activation energy analysis confirmed $Ea_{inh} = 59.4\ kJ\ mol^{-1} > Ea_{blank} = 43.8\ kJ\ mol^{-1}$, establishing that the adsorbed *XEL-B* film erects a kinetic energy barrier that substantially retards the electrochemical dissolution of iron in acidic media. Furthermore, Random Forest machine learning independently corroborated the ANOVA findings, ranking inhibitor concentration as the dominant process variable (IE: 77.54%; Rc: 74.20%), followed by immersion time (IE: 12.01%; Rc: 11.80%) and temperature (IE: 10.45%; Rc: 14.00%), with Gradient Boosting cross-validation confirming concordant rankings. This provided a data-driven basis for prioritising inhibitor dosage as the primary lever in field deployment optimisation. Collectively, these findings position *XEL-B* as a promising, biodegradable, and cost-effective alternative to conventional synthetic corrosion inhibitors in dilute acid service environments. Future work will encompass electrochemical impedance spectroscopy, potentiodynamic polarisation measurements, and density functional theory (DFT) molecular orbital calculations on *XEL-B* phytoconstituent adsorption geometries on Fe(110) surfaces to further elucidate the electronic and molecular mechanisms underlying the observed inhibition performance.

REFERENCES

1. Adesina, O. S., Ogundipe, O. B., Ajewole, J. B., Sanyaolu, O. O., Durugbol, J., Adekanye, T. A., Olabanji, T. S., Alao, O. P., & Dada, T. J. 2025. Corrosion Challenges, Monitoring Techniques, and Mitigation Strategies in The Oil and Gas Industry: A Critical Review. Journal of Science and Technology Research,7, pp. 267–278.
2. Alamiery, A. A., Isahak, W. N. R. W., Aljibori, H. S. S., Al-Asadi, H. A., & Kadhum, A. A. H. (2021). Effect of the structure, immersion time and temperature on the corrosion inhibition of 4-pyrrol-1-yl-N-(2,5-dimethyl-pyrrol-1-yl)benzoylamine in 1.0 M HCl solution. International Journal of Corrosion and Scale Inhibition, 10(2), 700–713. https://doi.org/10.17675/2305-6894-2021-10-2-14

ISSN 2278-2540 | DOI: 10.51583/IJLTEMAS | Volume XV, Issue III, March 2026

3. Alao, A. O., Popoola, A. P., Dada, M. O., & Sanni, O. (2022). Utilization of green inhibitors as a sustainable corrosion control method for steel in petrochemical industries: A review. Frontiers in Energy Research, 10, Article 1063315. https://doi.org/10.3389/fenrg.2022.1063315
4. Al Otaibi, N., & Hammud, H. H. (2021). Corrosion inhibition using Harmal leaf extract as an eco-friendly corrosion inhibitor. Molecules, 26(22), 7024. https://doi.org/10.3390/molecules26227024
5. Al-Baghdadi, S., Gaaz, T. S., Al-Adili, A., Al-Amiery, A. A., & Takriff, M. S. (2021). Experimental studies on corrosion inhibition performance of acetylthiophene thiosemicarbazone for mild steel in HCl complemented with DFT investigation. International Journal of Low-Carbon Technologies, 16(1), 181–188. https://doi.org/10.1093/ijlct/ctaa050
6. Bandeira, R. M., Lima, F. P., Nunes, M. S., dos Santos, E. C., dos Santos Júnior, J. R., de Matos, J. M. E., Feitosa, C. M., Rai, M., Bhattarai, S., & Das Mulmi, D. (2025). The green plant-based corrosion inhibitors—a sustainable strategy for corrosion protection. Surface Science and Technology, 3, Article 19.https://doi.org/10.1007/s44251-025-00019-x
7. Barbu, C. A., Fierascu, I., Semenescu, A., & Cotrut, C. M. (2025). Critical Review Regarding the Application of Plant Extracts as Eco-Friendly Corrosion Inhibitors—A Sustainable Interdisciplinary Approach. Molecules, 30(18). https://doi.org/10.3390/molecules30183722
8. Cappelli, F., Castronuovo, G., Grimaldi, S., & Telesca, V. (2024). Random Forest and Feature Importance Measures for Discriminating the Most Influential Environmental Factors in Predicting Cardiovascular and Respiratory Diseases. International Journal of Environmental Research and Public Health, 21(7), 867. https://doi.org/10.3390/ijerph21070867
9. Iroha, N.B., Akaranta, O. Experimental and surface morphological study of corrosion inhibition of N80 carbon steel in HCl stimulated acidizing solution using gum exudate from Terminalia Mentaly, 2020. SN Applied Sciences, 2(1514). https://doi.org/10.1007/s42452-020-03296-8
10. Ituen, E., Singh, A., Yuanhua, L., & Akaranta, O. (2021). Biomass-mediated synthesis of silver nanoparticles composite and application as green corrosion inhibitor in oilfield acidic cleaning fluid. Cleaner Engineering and Technology, 3, 100119. https://doi.org/10.1016/j.clet.2021.100119
11. Kania, H., 2023. Corrosion and Anticorrosion of Alloys/Metals: The Important Global Issue. Coatings, 13(2), https://doi.org/10.3390/coatings13020216
12. Kumari, P., & Lavanya, M. (2022). Plant extracts as corrosion inhibitors for aluminum alloy in NaCl environment - Recent review. Journal of the Chilean Chemical Society, 67(2). https://doi.org/10.4067/S0717-97072022000205490
13. Mohammad, A. & Jafar, M., 2020. Global Impact of Corrosion: Occurrence, Cost and Mitigation. Global Journal of Engineering Science. 5(4): https://doi.org/10.33552/GJES.2020.05.000618
14. Yuan, X., Liu, S., Feng, W. & Dauphin, G., 2023, Feature Importance Ranking of Random Forest-Based End-to-End Learning Algorithm. Remote Sensing, 15, 5203. https://doi.org/10.3390/rs15215203
15. Zakeri, A., Bahmani, E., & Sabour Rouh Aghdam, A. (2022). Plant extracts as sustainable and green corrosion inhibitors for protection of ferrous metals in corrosive media: A mini review. Corrosion Communications, 5, 25–38. https://doi.org/10.1016/j.corcom.2022.03.002